Investigation of a New Macroscopic Model of Tra□c Flow

Kate Alexander

Abstract

The study of tra□c flow as given rise to many models aiming to realistically predict the behaviour of tra□c. Here we discuss a macroscopic method, closely related to the Bando [1] microscopic model. A similarity solution is found for the inhomogeneous case and the homogeneous case is solved for a Riemann problem. We use Roe decomposition with the first order upwind scheme to find a numerical solution and investigate the e□ect of the source and relaxation terms on the system.

Declaration

I confirm that this is my own work and the use of all materials from other sources has been properly and fully acknowledged.

Signed

Acknowledgements

I would like to thank my supervisors Professor Mike Baines and Dr Peter Sweby for their help with this project. I am very grateful for all their encouragement, endless patience and for Mike's fabulous sense of humour. I am also very grateful to Sue Davis, Jo Morgan and my fellow M.Sc. students for their support.

I would also like to thank the EPSRC for their financial support throughout this course.

Contents

1 Introduction 1

2 Traffic Models 3

2.1 Microscopic Models 3

2.1.1 The Bando Model 4

2.2 Macrosopic Models 5

2.2.1 The BMW Model 7

3 A New Macroscopic Model 11

3.1 A Similarity Solution 12

4 The Homogeneous System 16

4.1 The Riemann Solution 18

4.1.1 Different Initial Data 23

5 The Numerical Method 25

5.1 Roe Decomposition 25

5.2 The Roe Scheme 28

5.2.1 Accuracy and Stability 28

5.2.2 Boundary Conditions 29

5.3 The Data 29

6 Numerical Results 30

6.1 The Homogeneous System 30

6.2 The Inhomogeneous System 32

6.2.1 Constant $\bar{V}$ 32
6.2.2 Function $\bar{V}(\eta)$ 33
6.3 The Similarity Solution 34

7 Conclusions and Further Work 37

Chapter 1

Introduction

Much interest has been focused on traffic flow models over the last few decades as the amount of traffic on the roads continues to increase. Congestion is becoming more of a problem and as a consequence the accident rate is also increasing. Today there exist many schemes which not only aim to safely control the traffic but also to maximise its flow. Consider, for example, the variable speed limits on motorways. Information of the amount of vehicles and the traffic conditions on the road is recorded and the speed restrictions altered accordingly. Such schemes depend on the realistic modelling of the flow of traffic, given certain road conditions, in order to accurately predict the behaviour of the traffic over time.

Similarities can be drawn between the flow of traffic and that of a shallow fluid and as such many models have been based on the shallow water equations. Chapter 2 describes some of these models and outlines the drawbacks of such an assumption. Furthermore, we see in Section 3.1 that granular avalanche flow can be described by similar means, and we can apply some of the techniques involved in this field to our traffic model. Chapter 2 continues with the derivation of the continuum BMW [5] model from the car-following Bando [1] model.

In Chapter 3 we derive an alternative continuum model and, by introducing a moving coordinated system, we find a similarity solution to the system.

The behaviour of this solution, as time increases, is discussed and we later use this information as a comparison to our numerical scheme.

In Chapter 4 we consider the homogeneous system. Given sets of initial data with a single discontinuity we solve the Riemann problem of the homogeneous system to determine the behaviour and type of discontinuity.

Chapter 5 develops the First Order Upwind Scheme with Roe decomposition and we use the results of the Riemann problem to compare the programs output for the homogeneous system. The results for the homogeneous system and the inhomogeneous system, including the similarity solution, follows in Chapter 6.

Lastly, we draw conclusions on the method from the numerical results and suggest improvements and areas of further study.

Throughout the text we take the word *car* to be synonymous with *vehicle*.

2.1.1 The Bando Model

In 1995 Bando *et al*. [1] published a paper on *The Dynamical Model of Tra c Congestion and Numerical Simulation* which aims to model the "*d56656*"

Both models are studied with the initial data $L = 200$ and $N = 100$ where L is the length of the circuit (assuming periodic boundary conditions) and N is the number of cars on the road, and $b = \frac{L}{N}$. This initial data produces a stable model. The conditions for stability are analysed in [1]. A small perturbation is introduced in the movement of the first vehicle and the solution is advanced with time. The model with the optimal velocity function (2.3) generates spontaneous congestion and appears to realistically describe actual traffic.

2.2 Macrosopic Models

Alternative models come from a continuum or macroscopic approach which is an Eulerian, fluid-like approach. These models describe the average velocity and density of the traffic at a point. Unlike the car-following method the movement of all the vehicles is described by two coupled partial differential equations (except for the LWR model, see below), and is therefore less computationally expensive to solve.

All continuum models consist of a conservation equation, namely

$$\rho_t + (\rho v)_x = 0; \tag{2.4}$$

where $v(x;t)$ is the velocity. The density $\rho(x;t)$ of the traffic is the mass of vehicles per kilometre at time t. This conservation equation conserves the mass of vehicles in the system which is dependent on the flow (flux) of cars entering, leaving and already in the system. It amounts to saying that vehicles cannot appear or disappear. The conservation of mass equation is then coupled with a second conservation of momentum equation (or dynamic equation) dependent on the characteristics of the traffic. The non-linearity of such a system automatically generates congestion given smooth initial data.

There are many macroscopic models that have been developed over the last fifty years. In 1955 Lighthill and Whitham published two papers on kinematic waves. The latter paper [2] models the traffic solely by the conservation law (2.4) where the velocity v is assumed to be a decreasing function of the

density ½. In the following year a similar paper was published by Richards independent of Lighthill and Whitham, and the single equation model,

$$½_t + (½V(½))_x = 0;$$

is known as the LWR model. Zhang [6], who gives a clear introduction to macroscopic modelling, states that the LWR model is capable of describing some features of tra□c such as vehicles approaching and leaving tra□c congestion where a *shock* forms, and the anisotropic nature of real tra□c. However, due to certain assumptions, the LWR model is incapable of describing other aspects of tra□c flow, in particular flow through narrow spaces (bottlenecks) or when the tra□c stops and starts.

In the 1970s Payne and Whitham [3] developed a di□erent approach to the macroscopic model. They drew similarities between the flow of tra□c and fluid and based their model on the Navier-Stokes equations of incompressible flow. The PW model is

$$v_t + vv_x = \frac{V(½) \; i \; v}{¿} \; i \; \frac{c(½)}{½}½_x \tag{2.5}$$

where ¿, the relaxation term, is the driver's reaction time, $V(½)$ is a velocity function of the density and $c(½)$ is an anticipation term as described in [8]. However, the PW model can give negative speeds allowing the cars to travel backwards. Also the assumption that tra□c flow is fluid-like does not agree with the anisotropic nature of physical tra□c flow. This is because fluid particles are *isotropic* and as such react equally to information from behind as well as from in front.

The following years saw several attempts to improve the PW model. Modifications have been made by, amongst others, Kerner and Konhäuser [4] who included a viscosity term to stop the formation of unrealistic shocks,

$$v_t + vv_x = \frac{V(½) \; i \; v}{¿} \; i \; \frac{c_0^2}{½}½_x + \, ¹\frac{v_{xx}}{½}; \tag{2.6}$$

and Zhang who replaced the constant, c_0^2 in (2.6) with the function $c(½)$ in order to solve the problem of negative velocities. These models all yield some

unrealistic traffic properties due to the close link with fluid flow. Aw and Rascle [7] develop a different second equation, Lagrangian in nature, in an attempt to overcome this problem.

2.2.1 The BMW Model

In 2000 Berg, Mason and Woods [5] (BMW) proposed a continuum model derived from the Bando car-following model (2.1) written in terms of the density ρ rather than the headway b. Usually the density is defined as

$$\rho = \frac{1}{b}. \tag{2.7}$$

Berg *et al.*, however, state that this definition is inaccurate. They consider the open interval $(1, y)$ with cars at positions $x = 1, 2, 4, 8, \ldots, n, \ldots$ so the car at the point x has a headway $b = x$.

Assuming that (2.7) holds, $\rho = \frac{1}{x}$ and thus the number of cars in the open interval $(1, y)$ is

$$\int_1^y \frac{1}{x}\,dx = \log_e y. \tag{2.8}$$

From the above diagram we see that the headway of car n is $b = y = 2^n$. Therefore, the number of cars in the interval is $n = \log_2 y$. Hence the assumption that $\rho = \frac{1}{b}$ is, in fact, incorrect by a factor of $\log_e 2$. As illustrated below, Berg *et al.* find an alternative definition relating the density to the headway by calculating a higher order approximation to $\rho(b)$.

Berg *et al.* state that a more accurate relation between ρ and b is

$$\int_{x_n}^{x_n+b} \rho(x, t)\,dx = 1,$$

for all i where x_i is the position of car i at a given time. They set up a consistent mapping between the positions of the vehicles, fx_ig, and their associated density function, $\rho(x)$. This mapping is not unique. However, given the position of the first car the inverse mapping is unique and it is this which is required to derive a macroscopic momentum equation from (2.1).

Considering all cars on a road, Berg *et al.* expand (2.8) as

Zn c t ion ,

and substituting in (3.8) to give

$$b \approx \frac{1}{\rho} - \frac{\rho_x}{2\rho^3} - \frac{\rho_{xx}}{6\rho^4} + \frac{\rho_x^2}{2\rho^5} \tag{2.12}$$

as an approximation to the headway in terms of the density.

Taking the derivative of (2.9) using Leibnitz's Rule gives the conservation equation (2.4) and hence v is consistent in the model. Equation (2.12) is then applied to the Bando model (2.1) using

$$\begin{aligned} V_B(b_n) &= V_B\left(\frac{1}{\rho} - \frac{\rho_x}{2\rho^3} - \frac{\rho_{xx}}{6\rho^4} + \frac{\rho_x^2}{2\rho^5}\right) \\ &= V_B\left(\frac{1}{\rho}\right) + -\frac{\rho_x}{2\rho^3} - \frac{\rho_{xx}}{6\rho^4} + \frac{\rho_x^2}{2\rho^5} V_B'\left(\frac{1}{\rho}\right) \\ &= \bar{V}(\rho) + \bar{V}'(\rho)\left(\frac{\rho_x}{2\rho} + \frac{\rho_{xx}}{6\rho^2} - \frac{\rho_x^2}{2\rho^3}\right); \end{aligned}$$

where $\bar{V}(\rho) = V_B\left(\frac{1}{\rho}\right)$ which gives a second dynamic equation of type (2.1) in the form

$$v_t + vv_x = a[\bar{V}(\rho) - v] + a\bar{V}'(\rho)\left(\frac{\rho_x}{2\rho} + \frac{\rho_{xx}}{6\rho^2} - \frac{\rho_x^2}{2\rho^3}\right); \tag{2.13}$$

to be coupled with (2.4). Here the pressure-like term ρ_x (cf. gas kinetics)

This chapter has given a brief insight to the car-following and continuum methods of tra□c modelling and, in particular, the derivation of the BMW model from the Bando model. In the next chapter we discuss a limitation in this derivation and consider a new conservation of momentum equation also based on the Bando model.

Substituting for v and replacing ¿ with t

$$\frac{@½}{@t} \; ¡ \; v_0 \frac{@½}{@»} + \frac{@(½\check{v})}{@»} + \frac{@(½v_0)}{@»} = 0$$

which reduces to

$$\frac{@½}{@t} + \frac{@(½\check{v})}{@»} = 0 \tag{3.5}$$

since v_0 does not depend on $»$.

We substitute for v in the second equation (3.2) of the system to give

$$\check{v}_t + v_{0t} + vv_x + v_0\check{v}_x = a(\bar{V} \; ¡ \; \check{v} \; ¡ \; v_0)$$

and, using the relation for v_{0t} above, this reduces to

$$\check{v}_t + \check{v}\check{v}_x + v_0\check{v}_x = \; ¡ \, a\check{v} + Cb_x:$$

After applying the transformation of variables (3.4)

$$\frac{@\check{v}}{@¿} \; ¡ \; \frac{@\check{v}}{@»}v_0 + \check{v}\frac{@\check{v}}{@»} + v_0\frac{@\check{v}}{@»} = \; ¡ \, a\check{v} + C\frac{@b}{@»}$$

and, again setting $¿ = t$,

$$\frac{@\check{v}}{@t} + \check{v}\frac{@\check{v}}{@»} \; ¡ \; C\frac{@b}{@»} + a\check{v} = 0: \tag{3.6}$$

To obtain a similarity solution we suppose that $\check{v}$ varies linearly with $»$, i.e. $\check{v} = »f(t)$ a185.446.42615such (3.6) becomes

$$»f' + »f^2 \; ¡ \; C\frac{@b}{@»} + a»f = 0: \tag{3.7}$$

Recall the conservation of mass equation after the change of variables (3.5)

$$\frac{@½}{@t} + \frac{@(½\check{v})}{@»} = 0:$$

We replace ½ by $\frac{1}{b}$ giving

$$\frac{@b}{@t} ¡ b\frac{@\check{v}}{@»} + \check{v}\frac{@b}{@»} = 0 \tag{3.9}$$

and then substituting in for b, given in (3.8), where

$$\frac{@b}{@t} = \frac{»^2}{2C}(f^{'} + f^2 + af)^{'} + b_0^{'}$$

and

$$\frac{@b}{@»} = \frac{»}{C}(f^{'} + f^2 + af);$$

we next make our substitution for $\check{v}$ to obtain (3.9) in the form

$$\frac{»^2}{2C}(f^{'} + f^2 + af)^{'} + b_0^{'} + \frac{f»^2}{2C}(f^{'} + f^2 + af) ¡ fb_0 = 0:$$

This holds for all » if

$$b_0^{'} = fb_0 \tag{3.10}$$

and

$$(f^{'} + f^2 + af)^{'} = ¡ f(f^{'} + f^2 + af) \tag{3.11}$$

Rewriting equation (3.10) in terms of ½$_0$ where $b_0 = \frac{1}{½_0}$ gives

$$½_0^{'} = ¡ f½_0 \tag{3.12}$$

which we substitute into (3.11) and integrating with respect to t, we arrive at

$$f^{'} = A½_0 ¡ f^2 ¡ af \tag{3.13}$$

where A is a positive constant of integration. This system of two ordinary di□erential equations has a fixed point at $(½; f) = (0; 0)$. We plot ½$_0$ against f to investigate their behaviour as time $t \to 1$. Hence we can deduce the behaviour of the system as time evolves.

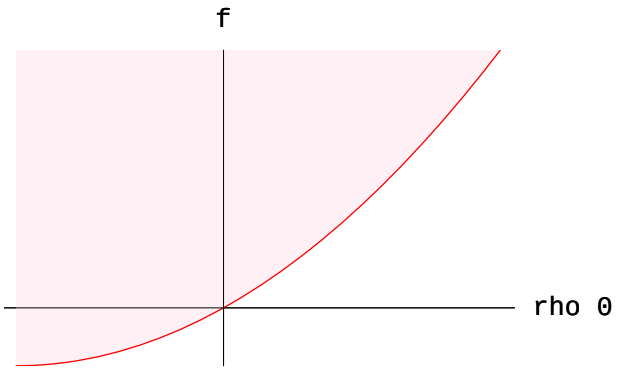

Figure 3.1: *Plot of* $f' = \frac{A}{\rho_0} - f^2 - af = 0$. *The shaded region indicates where* $f' < 0$.

Since both f and ρ_0 are positive $\frac{\rho_0}{\rho_0}$ is always negative. The shaded area in Figure 3.1 indicates the the

Chapter 4

The Homogeneous System

In this chapter we look at the case when $a = 0$. This homogeneous sub-problem of (3.2) is

$$\begin{aligned} \rho_t + (\rho v)_x &= 0 \\ v_t + v v_x &= C b_x \end{aligned} ; \tag{4.1}$$

where the zero relaxation term a means there is no source term $(\bar{V} - v)$. In Section 4.1 we find a solution to a Riemann problem of the system. In order to do this we start by writing the system in *conservation form*

and simplifying, we obtain

$$(\rho v)_t + (\rho v^2)_x = \rho a(\bar{V}(\rho) - v) + \rho C b_x.$$

We now assume that the usual relation between the density and the headway holds, i.e. $b = \frac{1}{\rho}$. Therefore, $b_x = -\frac{\rho_x}{\rho^2}$ and so $\rho b_x = (\ln \rho)_x$. Substituting this into the above g1is into thess

such that $(A - \lambda_k I)r_k = 0$, for $k = 1, 2$. The system is non-linear and, in general, an analytic solution of such is not possible. However, we can find an exact solution of the Riemann problem, consisting of initial data giving a single discontinuity between two constant states.

4.1 The Riemann Solution

We now consider the non-linear, homogeneous system (4.1) which gives $R = 0$ in the conservation form. The eigenvalues are real and distinct thus ensuring *strict hyperbolicity*.

Given the initial data at time $t = 0$

$$u = \begin{cases} u_L & x \leq 0 \\ u_R & x > 0 \end{cases}$$

there is a discontinuity at the origin. We decompose the initial discontinuity into n (here $n = 2$) separate waves between $n + 1$ constant states. Each new k-wave, with $k = 1, \ldots, n$ is one of the following three tyTD[((tinrl9(389296(one)-295(of)-2D[((tinrl(

$$\mathbf{u}_R = \begin{pmatrix} \rho_R \\ (\rho v)_R \end{pmatrix} = \begin{pmatrix} 0.6 \\ 0.09 \end{pmatrix}$$

where $0 \cdot x \cdot 30$ so the discontinuity lies at $x = 15$. This initial data is used in [8] to test the Riemann problem for the PW, Zhang and Aw and Rascle models. Here we have normalised ρ and v such that $\rho \in [0, 1]$ and $v \in [0, 1]$. The initial data models a situation where traffic travels from low density to high density, for example when approaching congestion.

The Rankine-Hugoniot jump condition is

$$\mathbf{f}(\mathbf{u}) - \mathbf{f}(\hat{\mathbf{u}}) = s(\mathbf{u} - \hat{\mathbf{u}}),$$

where the fixed state $\hat{\mathbf{u}}$ is either $\mathbf{u}_L$ or $\mathbf{u}_R$, $\mathbf{f}$ is the flux and s is the shock speed. Applying this to our system yields the two equations

$$\begin{aligned} \rho v - \hat{\rho}\hat{v} &= s(\rho - \hat{\rho}) \\ \rho v^2 + C\rho \ln \rho - \hat{\rho}\hat{v}^2 - C\hat{\rho} \ln \hat{\rho} &= s(\rho v - \hat{\rho}\hat{v}), \end{aligned}$$

giving shock speeds

$$s = \frac{\rho v - \hat{\rho}\hat{v}}{\rho - \hat{\rho}},$$

where v is given by solving the quadratic

$$(\rho v - \hat{\rho}\hat{v})^2 - (\rho v^2 + C\rho \ln \rho - \hat{\rho}\hat{v}^2 - C\hat{\rho} \ln \hat{\rho})(\rho - \hat{\rho}) = 0$$

whose solutions are either

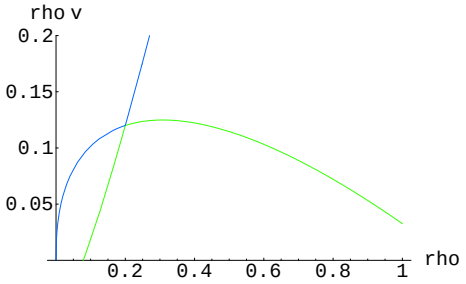

Figure 4.1: *The two curves given by (4.5) through u_L.*

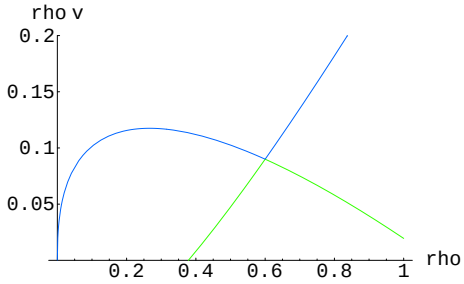

Figure 4.2: *The two curves given by (4.5) through u_R.*

will, therefore, ensure smooth Hugoniot curves by selecting the correct sign.

At each state, u_L or u_R, there are two possible Hugoniot curves. We require the k-Hugoniot curve, v_k, that is tangent to the k-eigenvector, r_k, at $\hat{u}$. Figures 4.3 and 4.4 show the two possible smooth Hugoniot curves and the eigenvector, r_k, at each end state $\hat{u}$. The red lines show the eigenvector, r_k, the green and blue lines show the Hugoniot curves where v takes the negative and positive signs respectively.

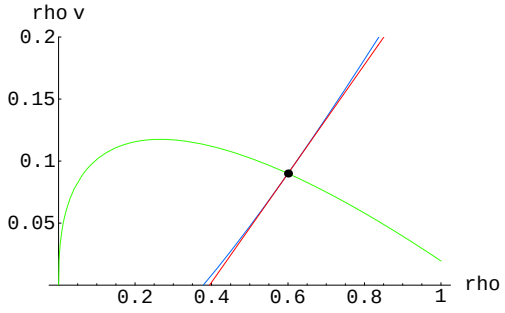

Figure 4.3: *The solid green line indicates the correct 1-Hugoniot curve which is tangent to the 1-eigenvector at u_L.h*

Figure 4.4: *The solid blue line indicates the correct 2-Hugoniot curve which is tangent to the 2-eigenvector at u_R.*

The 1-Hugoniot curve at u_L is

$$v_1 = \hat{v} - sgn(\cdot - \cdot)\sqrt{\frac{C(\ln\cdot - \ln\cdot)(\cdot - \cdot)}{\cdot\cdot}}$$

and at u_R the 2-Hugoniot curve is

$$v_2 = \hat{v} - sgn(\rho - \hat{\rho}) \sqrt{\frac{C(\ln\rho - \ln\hat{\rho})(\rho - \hat{\rho})}{\rho\hat{\rho}}}.$$

Since the two states do not lie on the same Hugoniot curve the discontinuity is not a single shock, but rather the end states u_L and u_R are connected by valid waves via u_M some intermediate state. In order for the Hugoniot curves to be valid we require the k-characteristic fields to be genuinely non-linear, that is

$$(\nabla_u \lambda_k) \cdot r_k(u) \neq 0$$

for all u. The system yields

$$(\nabla_u \lambda_1) \cdot r_1(u) = \left(\frac{1}{2}\sqrt{\frac{C}{\rho^3}}\right)\left(\frac{1}{\rho}\right) \cdot \begin{pmatrix} 1 \\ v - \sqrt{\frac{C}{\rho}} \end{pmatrix}^T = -\frac{1}{2}\sqrt{\frac{C}{\rho^3}}.$$

Similarly

$$(\nabla_u \lambda_2) \cdot r_2(u) = \frac{1}{2}\sqrt{\frac{C}{\rho^3}}$$

and hence it is genuinely non-linear. Incidently, if $(\nabla_u \lambda_k) \cdot r_k(u) = 0$ then we have a contact discontinuity. We now calculate where the Hugoniot curves are valid by using Lax's entropy condition at each constant end state

$$\lambda_1(u_L) > s > \lambda_1(u) \quad \text{and} \quad \lambda_2(u_R) < s < \lambda_R(u)$$

which holds for hyperbolic, genuinely non-linear conservation laws. Figures 4.5 an 4.6 are plots of $\lambda_k(\hat{u})$ (in red), s (in green) and $\lambda_k(u)$ (in blue). Figure 4.5 shows the 1-shock is entropy violating to the left of u_L, where the lines are dashed, and a valid shock to the right where the lines are solid. Figure 4.6 shows a similar situation for 2-shock at u_R.

We also find the k-Riemann invariants and thus the rarefactions/ simple waves at $\hat{u}$. The k-Riemann invariants are smooth functions $w_k(u)$ such that

$$\nabla_u w_k(u) \cdot r_k = 0$$

giving for the 1-shock

@ for 1 the rarefactions/ ^

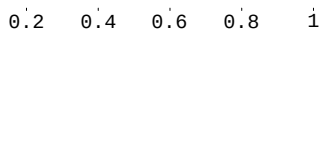

Figure 4.5: *The entropy condition holds to the right of u_L*

Figure 4.6: *The entropy condition holds to the right of u_R*

We seek solutions of (4.7) such that w_1 is constant on the characteristics, i.e.

$$\frac{d(\rho v)}{d\rho} - \frac{\rho v}{\rho} + \sqrt{\frac{C}{\rho}} = 0.$$

This is solved using the integrating factor $e^{\int \frac{1}{\rho} d\rho} = \frac{1}{\rho}$, to give the 1-Riemann invariant

$$w_1 = v - 2\sqrt{\frac{C}{\rho}}.$$

We can solve for v by setting

$$w_1 = v - 2\sqrt{\frac{C}{\rho}} = \text{constant} = \hat{v} - 2\sqrt{\frac{C}{\hat{\rho}}}$$

which gives v at u_L as

$$v_{w1} = \lambda_1(u_L) + 2\sqrt{\frac{C}{\rho}}.$$

Similarly the 2-Riemann invariant is

$$w_2 = v + 2\sqrt{\frac{C}{\rho}}$$

and v at u_R is given by

$$v_{w2} = \lambda_2(u_R) - 2\sqrt{\frac{C}{\rho}}.$$

isardses: and

In the figures below the rarefactions are represented by dashed curves and the shocks by solid curves. The 1-shock and v_{w1} are in green and the 2-shock and v_{w2} are in blue. The black points give the end states. Figure 4.9 shows the admissible rarefactions, given by v_{wk}, and shocks, v_k, and where they cross at u_M the red point. Figure 4.10 is an enlargement of the region containing u_M and u_L where Mathematica finds $u_M = (0.62 \quad 0.10)^T$. The left hand state u_L is connected to the right hand state, u_R by two Hugoniot curves which intersect at u_M.

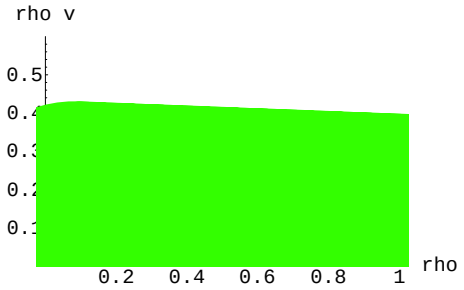

Figure 4.7: *The intersection of the valid Hugoniot curves and rarefaction waves connecting u_L to u_R via u_M.*

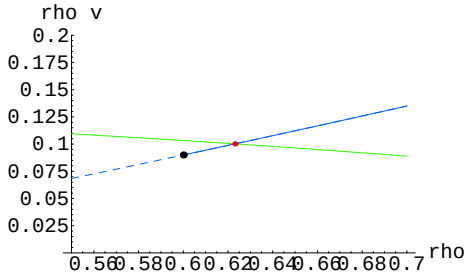

Figure 4.8: *Close up of the intersection at u_M.*

and) 4-332 (a7.97TfR7.47-99TD[(to)]TJ93]TJ687.97Tf20.51TD[(0)]A7.47-1.79T

4.1.1 Different Initial Data

We consider the situation where traffic moves away from congestion and high density towards lower density, for example when leaving a traffic jam or as traffic lights turn green. This circumstance uses the initial data where u_L and u_R are reversed, and so

$$u_L = \begin{matrix} 0 \\ @ \end{matrix}$$ *½TJ/F211.95T*

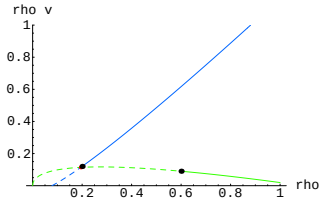

Figure 4.9: *The intersection of the valid Hugoniot curves and rarefaction waves connecting u_L to u_R via u_M.*

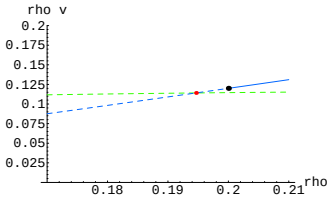

Figure 4.10: *Close up of the intersection at u_M.*

Chapter 5

The Numerical Method

Recall (4.4) giving the Jacobian matrix A, we set

$$\tilde{A} = \begin{pmatrix} 0 & 1 \\ \frac{C}{\rho} - \tilde{v}^2 & 2\tilde{v} \end{pmatrix}$$

where we assume $\widetilde{v^2} = \tilde{v}^2$ and find expressions for the averages $\tilde{v}$ a
terms of v and ρ. The method considers average values, denoted
which satisfy the discrete system taken in each cell. These average
unique and therefore the above assumption need not hold. It can,
be shown to be correct for our system. Equation (5.1) then gives

$$\Delta(\rho v) = \Delta(\rho v)$$

and

$$\left(\frac{C}{\rho} - \widetilde{v^2}\right)\Delta\rho + 2\tilde{v}\Delta(\rho v) = \Delta(\rho v^2 + C\ln\rho).$$

The second equation holds if

$$\frac{C}{\rho}\Delta\rho = C\Delta(\ln \rho\dot{v}\tilde{v})$$

/F31923TJ/F411.95Tf-1.1TJ/923TJ/TD[(2)]TJ/F27.5114.21630TD[(9Tf9.53056)]T3-

Expanding $(\sqrt{\rho_R}v_R \; i \; \sqrt{\rho_L}v_L)$ and taking the negative root we obtain

$$\tilde{v} = \frac{\sqrt{\rho_R}v_R \; i \; \sqrt{\rho_L}v_L}{\sqrt{\rho_R} + \sqrt{\rho_L}}:$$

Next we seek the Roe averages α_k and $\tilde{\lambda}_k$ where $k = 1; 2$, such that

$$\Delta u = \Sigma_{k=1}^{2} \alpha_k \tilde{r}_k \quad \text{and} \quad \Delta f = \Sigma_{k=1}^{2} \alpha_k \tilde{\lambda}_k \tilde{r}_k \tag{5.3}$$

and the right hand side vector

$$R(u) = \Sigma_{k=1}^{2} \tilde{\lambda}_k r_k \tag{5.4}$$

where

$$R(u) = \begin{pmatrix} 0 \\ a\rho(\bar{V}(\rho) \; i \; v) \end{pmatrix}$$

and $\lambda_k = \tilde{v}_i^{+} \sqrt{\frac{\bar{C}}{\rho}}$ are the eigenvalues and $r_k = \begin{pmatrix} 1; & \tilde{\lambda}_k \end{pmatrix}^T$ are the corresponding eigenvectors. From the first equation of (5.3) we obtain

$$\alpha_1 + \alpha_2 = \Delta\rho$$

and

$$(\alpha_1 + \alpha_2) + (\alpha_2 \; i \; \alpha_1) \sqrt{\frac{\bar{C}}{\rho}} = \Delta\rho v:$$

Therefore, the α_k T

5.2 The Roe Scheme

The first order upwind scheme with Roe decomposition is known as the Roe scheme. A numerical scheme approximates the solution to a problem in ($x; t$

cars approach from behind and must slow down sooner, thus we see the congestion (high density) propagates backwards along the road. As the cars enter the congested region the density increases slightly, where drivers 'ease o□' on the brakes, so deceleration is slower, and thus the headway of the cars approaching from behind decreases. The cars then slow down to the lower constant velocity. At the right hand end all the cars are travelling at a low speed because the headway is small.

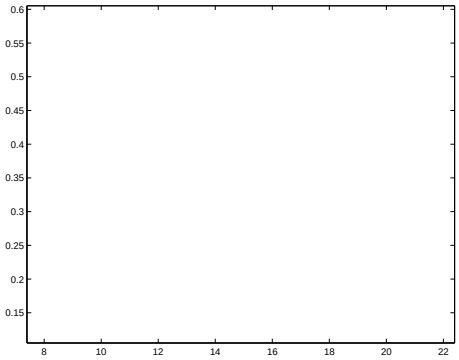

Figure 6.1: $a = 0$; $\Delta x = 0.1$, $\Delta t = 0.001$. *Every* 200^{th} *time step to* $t = 1$:

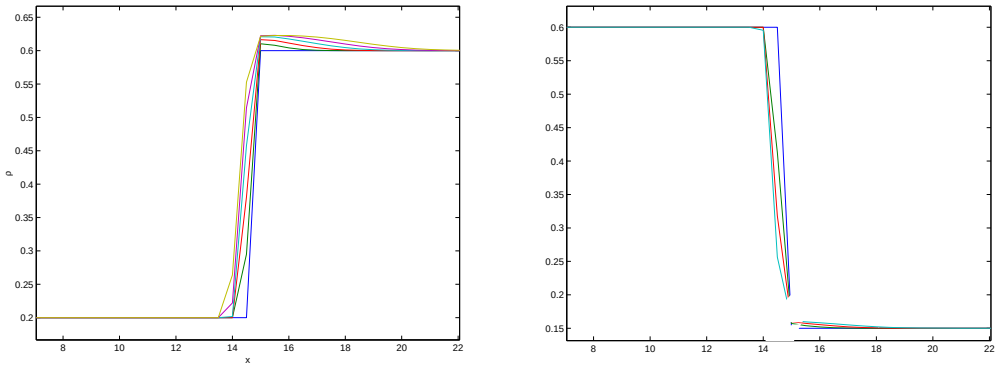

Figure 6.2: $a = 0$, $\Delta x = 0.5$, $\Delta t = 0.01$. *Every* 200^{th} *time step to* $t = 10$:

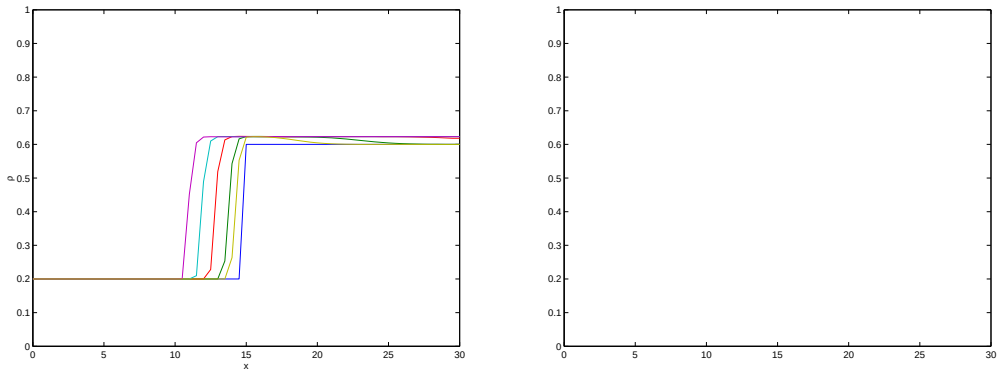

Figure 6.3: $a = 0$; $\Delta x = 0.5$; $\Delta t = 0.01$. *Every* 2000^{th} *time step to* $t = 100$.

6.2 The Inhomogeneous System

Now we consider the inhomogeneous system

$$\begin{aligned} \rho_t + (\rho v)_x &= 0 \\ v_t + v v_x - C b_x &= a(\bar{V}(\rho) - v). \end{aligned}$$

We run two programs, one where $\bar{V}$ is constant and the second where it is a function of ρ.

6.2.1 Constant $\bar{V}$

The program was run with $\Delta t = 0.01$ for 1000 time steps and various values of $\bar{V}$ and a. Figure 6.4, where $a = 0.1$; $\bar{V} = 0.9$ and $\Delta x = 0.3$ (therefore, only 60 space steps), shows the constant velocity to the left of the discontinuity increasing with time as cars here can accelerate, uniformly in space, with each time step to the optimal velocity, $\bar{V}$, since there is no change in the headway. Here the density is low and so the headway is large. When the vehicles reach the congestion they decelerate rapidly as before. Now, however, the density does not propagate backwards. The cars at the right hand state increase their constant velocity, with each time step, towards $\bar{V}$ The cars behind these adjust their speed and start to accelerate to reach the

same velocity. This causes the region of high density to move forward with each time step.

Figure 6:5 refines the space step size of the previous figures and gives a smoother representation. Figure 6:6 is the case when $a = 0{:}5$ and so the source term has a larger e□ect on the solution. The density behaves like the previous situation after a large time, as we would expect. The smooth

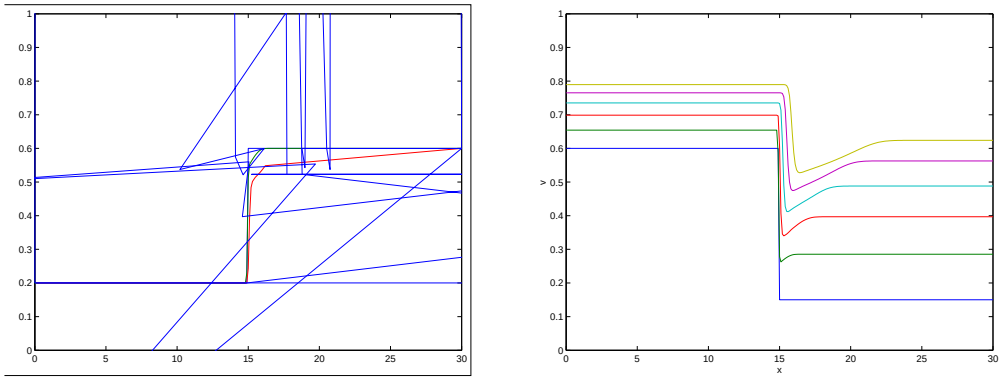

Figure 6.5: $a = 0.1$, $\bar{V} = 0.9$; $\Delta x = 0.1$, $\Delta t = 0.01$. *Every* 200^{th} *time step to* $t = 10$:

Figure 6.6: $a = 0.5$; $\bar{V} = 0.9$; $\Delta x = 0.3$; $\Delta t = 0.01$. *Every* 200^{th} *time step to* $t = 10$:

has been normalised and so ½ < 1 is not a physically possible solution. As a increase the maximum values of v and ½ do also.

6.3 The Similarity Solution

We run the inhomogeneous program with $x = »$ and $v = \check{v}$. This gives the system

$$\begin{aligned} ½_t + (½v)_» &= 0 \\ v_t + v\check{v}_» \ ¡ \ Cb_» &= a(\bar{V} \ ¡ \ \check{v}) \end{aligned}$$

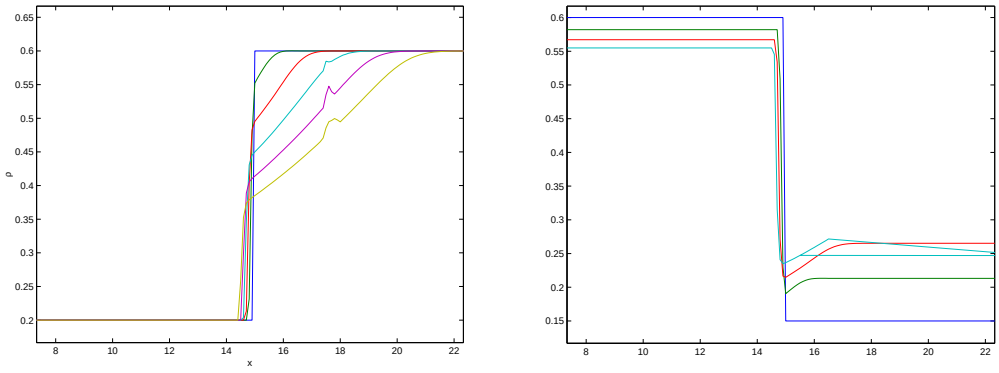

Figure 6.7: $a = 0.1$; $\bar{V} = 0.5$; $\Delta x = 0.3$; $\Delta t = 0.01$. *Every* 200^{th} *time step to* $t = 10$:

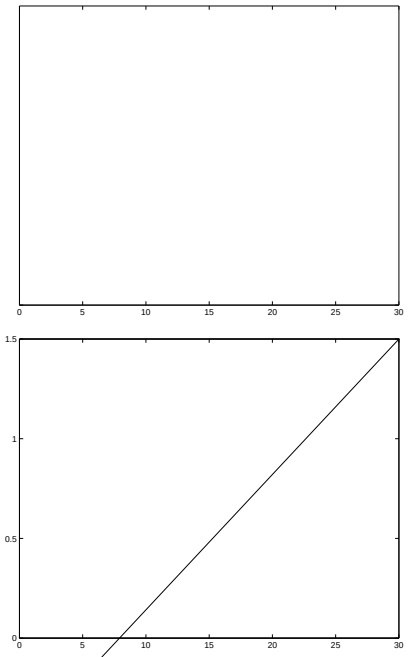

Figure 6.8: $a = 0.1$; $\bar{V} = 0.9$; $\Delta x = 0.3$; $\Delta t = 0.01$. *Every* 200^{th} *time step to* $t = 10$:

and setting $\bar{V} = 0$ we can compare the results with the similarity solution.

In Figure 6.9 we see that given any initial data the solution of $\check{v}$

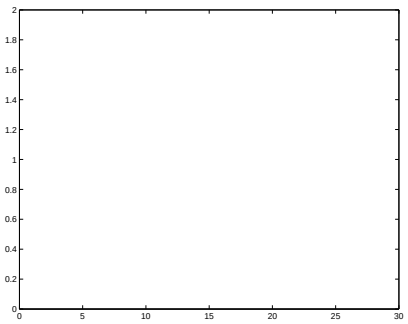

Figure 6.9: $a = A = 1$; $\bar{V} = 0$; $\Delta» = 0{:}1$; $\Delta t = 0{:}01$. *Every* 200^{th} *time step to* $t = 10$:

Chapter 7

Conclusions and Further Work

The aim of this dissertation has been to develop a macroscopic traffic flow model from a microscopic model and to solve it numerically. We based our dynamic equation on Bando [1] and introduced an extra term governing change in the headway.

A moving coordinate system is used to find a similarity solution to the inhomogeneous model. The behaviour of the solutions approach the fixed point $(\rho_0, f) = (0, 0)$ as $t \to 0$. Thus the source term has a large effect on the model causing the speed of the cars to approach the optimal velocity $\bar{V}$. These results are also given by the numerical method.

The homogeneous system is considered with initial data giving a single

istically the optimal velocity *is* dependent on the density. Since, in constant density, it would be foolhardy to drive at the same optimal velocity for congested tra□c as one would in light tra□c flow.

Another refinement is to assume that C is also a function of the density ½ and to develop a system that switches between two sub-problems at a defined value of the headway. By these means we would hope to model the way the tra□c accelerates in low density and maintains a lower steady speed in high density.

Bibliography

[1] M.Bando *et al.*, *Dynamical model of tra c congestion and numerical*

[10] Y.C. Tai, S. Noelle, J.M.N.T. Gray & K. Hunter *Shock-Capturing and Front-Tracking Methods for Granular Avalanches* Journal of Computational Physics 175, pp269 ¡ 301 (2001)

[11] R.J. Leveque *Finite Volume Methods for Hyperbolic Problems* Cambridge University Press (2002)

[12] P.K.Sweby *Numerical Techniques for Conservation Laws* course notes for M.Sc. module, (2003)